Co-planar Stereotactic Atlas of the Human Brain: 3-Dimensional Proportional System. An Approach to Cerebral Imaging (Thieme, Stuttgart, 1988)], followed by nonlinear deformation to match a template brain. These registration procedures are based on an automatic, multiscale feature-matching algorithm [D. L. Collins, C. J. Holmes, T. M. Peters, A. C. Evans, *Hum. Brain Mapp.* **3**, 190 (1995)]. Subsequently, a binary white matter mask was generated for each subject by means of an automatic tissue-classification algorithm. This algorithm is based on classification that uses an artificial neural network classifier (*25*). For each individual T_1-weighted image, we trained the algorithm by providing the stereotactic coordinates of brain regions (voxels) with a minimal 90% likelihood of being gray matter, white matter, or cerebrospinal fluid [A. Zijdenbos *et al.*, *Proceedings of the 4th International Conference on Visualization in Biomedical Computing*, K. H. Hohne and R. Kikinis, Eds. (Springer, Berlin, 1996), pp. 439–448; V. Kollokian, thesis, Concordia University, Montreal (1996)]. The white matter masks obtained in this way were blurred using a Gaussian smoothing kernel (full width at half-maximum, 10 mm); such a smoothing process averages the binary (0 or 1) values of neighboring voxels in 3D space, thus increasing signal-to-noise ratio. The voxel values in the resulting blurred white matter masks are referred to as white matter density (*6*).

9. The data set consisted of 111 pairs of normalized white matter density volumes and age (years) obtained from the 111 subjects. The significance of the relation between age and white matter density was assessed for each of the 3D volume elements (voxels) constituting a volume by means of simple linear regression [R. R. Sokal and F. J. Rohlf, *Biometry* (Freeman, San Francisco, 1981)]. The parameter of interest was the slope of the effect of age on white matter density, after removing the effect of gender. An estimate of the slope and its standard deviation were obtained by least-squares fitting of the linear model at each voxel; *t* values were calculated by dividing the voxel slope-estimate by its standard deviation. The resulting *t*-statistic map tested whether, at a given voxel, the slope of the regression was significantly different from zero. The presence of a significant peak was assessed by a method based on 3D Gaussian random-field theory, which corrects for the multiple comparisons involved in searching across a volume [K. J. Worsley *et al.*, *Hum. Brain Mapp.* **4**, 58 (1996)]. Values equal to or exceeding a criterion of $t = 5.0$ were considered as significant ($df = 108$, $P < 0.04$, two-tailed, corrected for whole-brain search).
10. We reanalyzed the data after excluding the 11 left-handed or ambidextrous subjects. The results were not different from those obtained in the original ($n = 111$) sample.
11. These negative findings should be treated with caution, however. Meaningful correlational analysis of this kind would require administration of a more comprehensive set of neuropsychological tasks known to tap various well-defined brain circuits, such as tests of fine motor skills and phoneme discrimination.
12. J. A. Eyre, S. Miller, V. Ramesh, *J. Physiol.* **434**, 441 (1991).
13. Human subjects: (*12, 26*); K. Muller, V. Homberg, H.-G. Lenard, *Electroencephalogr. Clin. Neurophysiol.* **81**, 63 (1991); A. Nezu *et al.*, *Brain Dev.* **19**, 176 (1997). Monkeys: E. Olivier, S. A. Edgley, J. Armand, R. N. Lemon, *J. Neurosci.* **17**, 267 (1997).
14. D. G. Lawrence and D. A. Hopkins, *Brain* **99**, 235 (1976); H. Forssberg, A. C. Eliasson, H. Kinoshita, R. S. Johansson, G. Westling, *Exp. Brain Res.* **85**, 451 (1991); J. Armand, E. Olivier, S. A. Edgley, R. N. Lemon, in *Hand and Brain: The Neurophysiology and Psychology of Hand Movements*, A. M. Wing, P. Haggard, J. R. Flanagan, Eds. (Academic Press, San Diego, CA, 1996), pp. 125–145; (*26*).
15. W. I. McDonald and T. A. Sears, *Brain* **93**, 583 (1970); H. A. Swadlow, *J. Neurophysiol.* **54**, 1346 (1985); P. Shrager, *Brain Res.* **619**, 278 (1993).
16. P. Tallal, S. Miller, R. H. Fitch, *Ann. N.Y. Acad. Sci.* **682**, 27 (1993); P. Belin *et al.*, *J. Cogn. Neurosci.* **10**, 536 (1998).
17. V. B. Penhune, R. J. Zatorre, J. D. MacDonald, A. C. Evans, *Cereb. Cortex* **6**, 661 (1996).
18. J. Moore, Y. Guan, B. J. Wu, *Assoc. Res. Otolaryngol. Abstr.* **20**, 28 (1997).
19. F. Boller and P. Marcie, *Neuropsychologia* **16**, 521 (1978); A. M. Liberman and I. G. Mattingly, *Cognition* **21**, 1 (1985).
20. P. Muller-Preuss and D. Ploog, *Brain Res.* **215**, 61 (1981); O. Creutzfeldt, G. Ojemann, E. Lettich, *Exp. Brain Res.* **77**, 476 (1989); T. Paus, D. W. Perry, R. J. Zatorre, K. J. Worsley, A. C. Evans, *Eur. J. Neurosci.* **8**, 2236 (1996).
21. Iron contained in oligodendrocytes is believed to play an important role in myelogenesis and the maintenance of myelin sheath [J. R. Conner and S. L. Menzies, *Glia* **17**, 83 (1996)]. Proton magnetic relaxation times are known to vary as a function of iron concentration [J. Vymazal *et al.*, *Magn. Reson. Imaging* **36**, 56 (1996); J. Vymazal, O. Zak, J. W. M. Bulte, P. Aisen, R. A. Brooks, *ibid.*, p. 61] such that a positive correlation can be expected between T_1-weighted signal and iron concentration in a given brain region. In light of the known age-related increases of the non-hemin iron in the human brain [B. Hallgren and P. Sourander, *J. Neurochem.* **3**, 41 (1958)], our findings could also reflect a gradual iron enrichment of white matter oligodendrocytes during childhood and adolescence.
22. R. Ilmonierni *et al.*, *Neuroreport* **8**, 3537 (1997).
23. T. M. Hyde, J. C. Ziegler, D. R. Weinberger, *Arch. Neurol.* **49**, 401 (1992).
24. J. N. Giedd *et al.*, *Dev. Brain Res.* **91**, 274 (1996).
25. M. Ozkan, B. M. Dawant, R. J. Maciunas, *IEEE Trans. Med. Imaging* **12**, 534 (1993).
26. K. Muller and V. Homberg, *Neurosci. Lett.* **144**, 57 (1992).
27. G. Schaltenbrand and P. Wahren, *Introduction to Stereotaxis with an Atlas of the Human Brain, Volume II* (Thieme, Stuttgart, 1977); P. St.-Jean *et al.*, *IEEE Trans. Med. Imaging* **17**, 672 (1998).
28. Supported in part by the International Consortium for Brain Mapping and the Medical Research Council (Canada). We thank G. Leonard, B. Milner, and R. Zatorre for comments on the manuscript and K. Velikonja for help with data analysis.

1 December 1998; accepted 19 February 1999

Signaling of Cell Fate Decisions by *CLAVATA3* in *Arabidopsis* Shoot Meristems

Jennifer C. Fletcher,[1] Ulrike Brand,[2] Mark P. Running,[1]* Rüdiger Simon,[2] Elliot M. Meyerowitz[1]†

In higher plants, organogenesis occurs continuously from self-renewing apical meristems. *Arabidopsis thaliana* plants with loss-of-function mutations in the *CLAVATA (CLV1, 2,* and *3)* genes have enlarged meristems and generate extra floral organs. Genetic analysis indicates that *CLV1*, which encodes a receptor kinase, acts with *CLV3* to control the balance between meristem cell proliferation and differentiation. *CLV3* encodes a small, predicted extracellular protein. *CLV3* acts nonautonomously in meristems and is expressed at the meristem surface overlying the *CLV1* domain. These proteins may act as a ligand-receptor pair in a signal transduction pathway, coordinating growth between adjacent meristematic regions.

The shoot apical meristem (SAM) is the source of all the aerial parts of the plant. Cells at the SAM summit serve as stem cells that divide slowly to continuously displace daughter cells to the surrounding peripheral region, where they are incorporated into differentiating leaf or flower primordia (*1*). A balance between creation of new meristematic cells by division and departure of cells from the meristem by differentiation is required to maintain a functional SAM. The *CLV3* and *CLV1* genes play critical roles in maintaining this balance, because loss-of-function mutations in either gene cause progressive SAM enlargement and floral meristem overgrowth (*2–6*). The phenotypes of representative wild-type and *clv3* mutant plants (*7*) are shown in Fig. 1. *CLV1* encodes a leucine-rich repeat (LRR) transmembrane receptor serine-threonine kinase (*8*). LRRs are a common motif of protein-binding domains (*9*), suggesting that CLV1 may bind an extracellular protein or peptide ligand. *clv1 clv3* double-mutant analysis shows that the genes are mutually epistatic (*5*), suggesting that the two gene products act in the same pathway. Doubly heterozygous (*clv1*/+; *clv3*/+) plants have a *clv* mutant phenotype (*5*), implying that the gene products have a quantitative interdependence, as if they acted together in a complex or in closely associated steps of a pathway. Thus, it appears that CLV3 protein acts either in the intracellular pathway leading from CLV1 activation to cellular activity, or in the production of, or as, the CLV1 ligand.

[1]California Institute of Technology, 1200 East California Boulevard, Pasadena, CA 91125, USA. [2]Institut für Entwicklungsbiologie, Universität zu Köln, Gyrhofstrasse 17, 50923 Köln, Germany.

*Present address: University of California Berkeley, U.S. Department of Agriculture–Agricultural Research Service Plant Gene Expression Center, 800 Buchanan Street, Albany, CA 94710, USA.

†To whom correspondence should be addressed at Division of Biology 156-29, California Institute of Technology, 1200 East California Boulevard, Pasadena, CA 91125, USA. E-mail: meyerow@cco.caltech.edu

To distinguish which hypothesis is correct, we cloned the *CLV3* gene using two tagged alleles, *clv3-3* and *clv3-7*. The *clv3-3* allele is caused by transferred DNA (T-DNA) integration (*10*) and confers a weak *clv3* phenotype, whereas the *clv3-7* allele is caused by integration of the maize transposable element *En-1* (*11*) and confers a strong phenotype. DNA sequence analysis of genomic clones flanking both insertion sites revealed the presence of three small, overlapping open reading frames (*12*). Comparison of the genomic clones with cDNA RACE products revealed a gene consisting of three exons and two small introns (Fig. 2).

The nucleotide and deduced amino acid sequence of *CLV3* is shown in Fig. 2. The *clv3-3* T-DNA insertion site lies 175 base pairs (bp) downstream of the polyadenylate [poly(A)] addition site (Fig. 2A), potentially disrupting an enhancer element. The *En-1* element in *clv3-7* inserted in the second intron, close to the intron–exon 3 boundary. The independently derived *clv3-1* and *clv3-5* ethylmethane sulfonate (EMS)–induced alleles have intermediate phenotypes and contain a G to A transition at position +266 relative to the translation initiation site (Fig. 2A) (*13*). The strong *clv3-2* γ ray–induced allele and the *clv3-4* x-ray–induced allele both contain breakpoints occurring between the Mfe I and Dra I restriction sites flanking the third exon (*14*), whereas the strong *clv3-6* EMS-induced allele alters the third exon splice acceptor site from AG to AA (Fig. 2A). Reversion of unstable *clv3-7* mutants to the wild-type phenotype was accompanied by loss of the *En-1* element, verifying that the gene cloned corresponds to *CLV3*.

The *CLV3* gene encodes a protein of 96 amino acids (Fig. 2B) that shows no appreciable similarity to other sequences or sequence motifs of known functional domains. An 18–amino acid NH_2-terminal hydrophobic region presumably acts as a signal peptide to direct the protein into the secretory pathway (*15*). No signals that would cause retention of the protein along the secretory pathway (*16*) were detected, indicating that the CLV3 protein may be extracellular and could therefore act as the ligand for the CLV1 receptor kinase. Alternatively, CLV3 could act to produce the ligand, function as a coligand with another small molecule, or assist CLV1 in ligand binding.

We investigated the cell autonomy of *CLV3* function using periclinal chimeras derived from the unstable *En-1*–induced *clv3-7* mutants. Secondary shoots on *clv3-7* plants that displayed a wild-type phenotype were isolated and allowed to self-pollinate. The progeny of these somatic revertants would segregate a wild-type (revertant) *clv3* allele if the reversion occurred in the L2 meristem cell layer that gives rise to the gametes (*17*), resulting in 75% wild-type progeny plants. Reversions occurring in the L1 or L3 layer would not be transmitted to the next generation, although secondary germinal reversion events (*18*) contribute to the appearance of up to 30% wild-type phenotypes among the otherwise *clv3* mutant progeny of L1 or L3 chimeras. Of 24 analyzed sectors, 11 segregated 0 to 30% wild-type plants, indicating that *CLV3* function was restored somatically in the L1 or L3 cell layer of the revertants, but not in the L2 (*19*). *CLV3* activity in one cell layer is therefore sufficient to control proliferation and differentiation across the entire meristem, possibly by communicating information across cell layers in a non–cell-autonomous manner.

The expression pattern of the *CLV3* gene during wild-type development was analyzed by RNA in situ hybridization (*20*). *CLV3* mRNA expression is first detected in heart stage embryos, in a patch of cells between the developing cotyledons (Fig. 3A) predicted to give rise to the SAM (*21*). In vegetative and inflorescence meristems, *CLV3* mRNA accumulates in a small zone of cells at the meristem apex (Fig. 3, B and C). It is expressed in the L1 and L2 cell layers, and in a few underlying L3 cells. *CLV3* signal is not detected on the shoot meristem flanks in cells of presumptive leaf and flower anlagen, but reappears in floral meristem apices at stage 2 (*22*). At stages 3 to 4, *CLV3* mRNA expression continues in the floral meristem central region (Fig. 3D) and persists there through stage 6, when the sepal primordia completely enclose the bud (*19*). Throughout development the RNA signal is always restricted to the most central, nondifferentiating meristem cells, the putative stem cells. The *CLV3* and *CLV1* (*6*, *23*) temporal expression patterns are very similar, but there are important spatial differences. *CLV1* mRNA, unlike *CLV3* mRNA, is not detected in the L1 cell layer of shoot or floral meristems, and *CLV1* is expressed more deeply in the L3 region than *CLV3* (compare Fig. 3E with Fig. 3D).

It has been postulated that the SAM enlargement observed in *clv1*, *clv2*, and *clv3* mutants (*3*, *5*, *6*) is due to central-zone expansion. Because *CLV3* mRNA coincides with the central zone, we used in situ hybridization to test this hypothesis. Inflorescence meristems of homozygous *clv1-4* plants (Fig. 4A) were hybridized to a *CLV3* probe, which showed that the *CLV3* expression domain is markedly expanded relative to the wild type (Fig. 4B). *CLV3* signal is detected throughout the enlarged shoot meristem, except for a narrow strip of cells closest to newly initiating floral primordia. A broadened *CLV3* expression domain is also observed in young *clv1-4* floral meristems (Fig. 4C). Although *CLV3* mRNA is undetectable in wild-type flowers after carpel initiation, it is present in more mature *clv1-4* flowers in a domain be-

Fig. 1. *clv3* shoot and flower phenotypes. (**A**) Wild-type inflorescence meristem. (**B**) *clv3-2* inflorescence meristems undergo fasciation, growing as a ring or line rather than a point. (**C**) *clv3-2* mutant flowers contain extra organs of all types, particularly stamens and carpels. Bars, 1 mm.

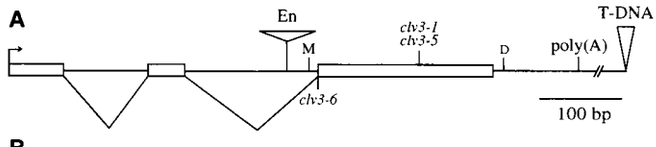

Fig. 2. *CLV3* genomic region and peptide sequence. (**A**) The *CLV3* genomic region. The translation start site is denoted by the arrow and the exons by boxes. The relative positions of the *clv3* mutations are shown. Restriction sites: M, Mfe I; D, Dra I. The genomic DNA sequence is available through GenBank under accession number AF126009. (**B**) The *CLV3* predicted amino acid sequence. Intron positions are indicated by arrows, the predicted signal sequence is underlined, and the amino acid altered in the *clv3-1* and *clv3-5* alleles is in bold type. Single-letter abbreviations for the amino acid residues are as follows: A, Ala; D, Asp; E, Glu; F, Phe; G, Gly; H, His; K, Lys; L, Leu; M, Met; N, Asn; P, Pro; Q, Gln; R, Arg; S, Ser; T, Thr; V, Val; and W, Trp.

tween the developing carpels (Fig. 4D). This domain gives rise to a nested fifth whorl ovary, containing cells that continue to proliferate and express *CLV3* even after the formation of ovules in the fourth whorl (Fig. 4E). Comparable enlargement of the *CLV3* expression domain is observed in *clv2-1* and *clv3-2* mutants, indicating that *CLV1*, *CLV2*, and *CLV3* all act to limit the number of cells in the *CLV3* expression domain. In situ hybridization also shows that the *CLV1* domain is enlarged in *clv1*, *clv2*, and *clv3* meristems proportionately to the enlargement of the *CLV3*-expressing domain (*6*, *24*).

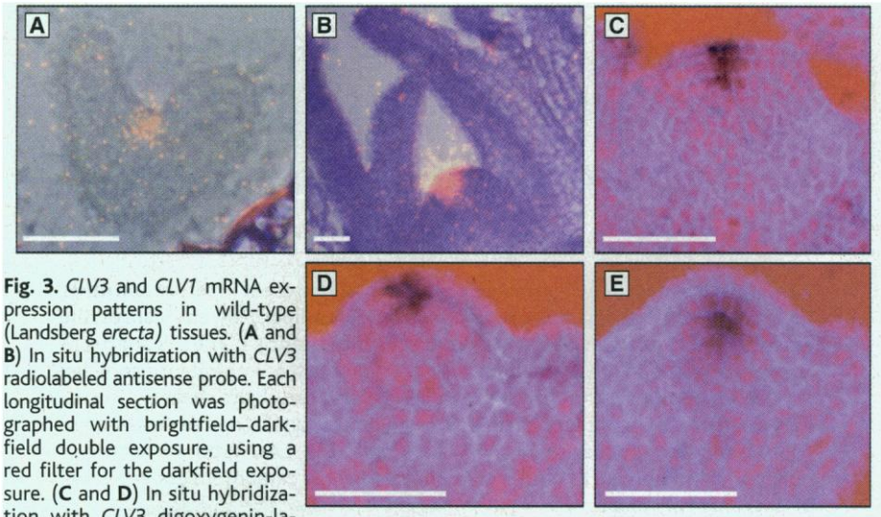

Fig. 3. *CLV3* and *CLV1* mRNA expression patterns in wild-type (Landsberg *erecta*) tissues. (**A** and **B**) In situ hybridization with *CLV3* radiolabeled antisense probe. Each longitudinal section was photographed with brightfield–darkfield double exposure, using a red filter for the darkfield exposure. (**C** and **D**) In situ hybridization with *CLV3* digoxygenin-labeled antisense probe. (**E**) In situ hybridization with *CLV1* digoxygenin-labeled antisense probe. (A) Heart stage embryo. (B) Ten-day-old seedling. (C) Inflorescence meristem. (D) Stage 3 flower. (E) Stage 3 flower. Bars, 50 μm. Control experiments with the sense strand of *CLV3* or *CLV1* detected no signal in tissue.

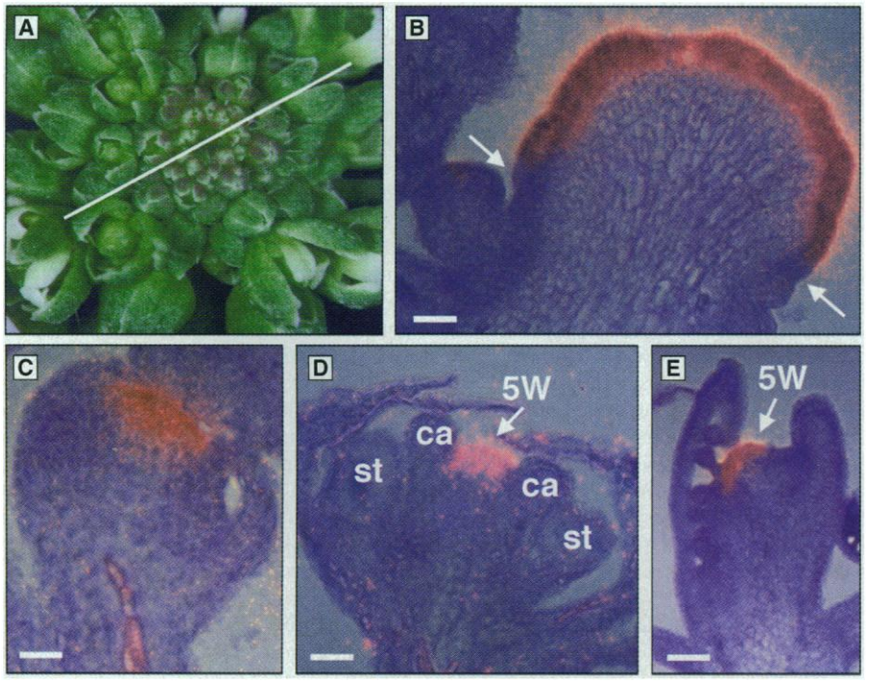

Fig. 4. *CLV3* mRNA expression patterns in *clv1* mutant tissues. (**A**) *clv1-4* inflorescence meristem and flowers. The line denotes the approximate orientation of the section taken in (B). (**B** to **E**) In situ hybridization with *CLV3* radiolabeled antisense probe. Each section was photographed with brightfield-darkfield double exposure, using a red filter for the darkfield exposure. (B) Abnormally enlarged *clv1* inflorescence meristem. *CLV3* is expressed throughout the enlarged meristem except at the margins (arrows). (C) Stage 5 *clv1* flower. (D) Stage 8 *clv1* flower. (E) Gynoecium of mature *clv1* flower. Abbreviations: st, stamen; ca, carpel; 5W, fifth whorl. Bars, 50 μm.

Loss of *CLV1*, *CLV2*, or *CLV3* activity causes accumulation of undifferentiated cells in the shoot apex, indicating that the *CLV* genes together promote the timely transition of stem cells into differentiation pathways, or repress stem cell division, or both. Loss of *CLV1* or *CLV3* activity also results in enlargement of the underlying *CLV1* domain. One hypothesis that fits these observations is that *CLV3* encodes a protein secreted from superficial cell layers in the central region, which acts as a ligand to activate the *CLV1* receptor kinase in underlying cells. The normal action of *CLV3* would be to repress enlargement of the *CLV1* domain. Because loss of *CLV1* or *CLV3* activity results in enlargement of the *CLV3* domain as well as the *CLV1* domain, one must infer that in addition to the size-repressing *CLV3/CLV1* pathway there is a size-enhancing, *CLV*-independent positive pathway from the underlying cells to the overlying ones that coordinates the size of the *CLV3* domain to match that of the *CLV1* domain. The net effect of the two pathways is to keep the relative sizes of the *CLV3* and *CLV1* domains fixed, allowing for meristem maintenance throughout the life of the plant. Disruption of the negative pathway, by mutating either *CLV3* or *CLV1*, results in enlargement of the *CLV1* domain, which in turn causes enlargement of the *CLV3* domain and progressive SAM enlargement.

CLV1 is a member of a plant-specific family of receptor protein kinases (*25*) that span the plasma membrane and allow cells to recognize and respond to their extracellular environment. CLV3 appears to be a ligand, or a molecule involved in ligand synthesis or binding, that is produced in one SAM region and acts on a receptor in another region, allowing for coordinated growth between them. The cloning of CLV3 thus allows a view of meristems as collections of intercommunicating cells, each synthesizing and secreting its own set of protein ligands and responding to its neighbors through action of its own complement of transmembrane receptor kinases. Such kinases are also common components of animal signal transduction pathways, although most developmentally important receptor protein kinases in animals are tyrosine kinases. Thus, plants and animals seem to have converged on independent but parallel mechanisms for sending similar sorts of signals, which can have profound effects on the development of the organisms.

References and Notes

1. T. A. Steeves and I. M. Sussex, *Patterns in Plant Development* (Cambridge Univ. Press, New York, 1989); E. M. Meyerowitz, *Cell* **88**, 299 (1997); S. E. Clark, *Sem. Cell Dev. Biol.* **7**, 873 (1996); P. Laufs, O. Grandjean, C. Jonak, K. Kieu, J. Traas, *Plant Cell* **10**, 1375 (1998).
2. H. M. O. Leyser and I. J. Furner, *Development* **116**, 397 (1992).
3. S. E. Clark, M. P. Running, E. M. Meyerowitz, *ibid.* **119**, 397 (1993).

4. J. Alvarez and D. R. Smyth, in Arabidopsis: *An Atlas of Morphology and Development*, J. L. Bowman, Ed. (Springer-Verlag, New York, 1994).
5. S. E. Clark, M. P. Running, E. M. Meyerowitz, *Development* **121**, 2057 (1995).
6. J. M. Kayes and S. E. Clark, *ibid.* **125**, 3843 (1998).
7. The *clv3-1* and *clv3-2* alleles have been described (*4*, *5*). The *clv3-3* allele was identified in line CS6421 from the Ohio State *Arabidopsis* Biological Resource Center. The *clv3-4* allele was isolated by G. Redei and donated to the Ohio State *Arabidopsis* Biological Resource Center under the designation CS3603. The *clv3-5* allele was identified in an EMS mutagenesis of *cuc2* mutant plants in the Landsberg *erecta* ecotype. The *clv3-6* allele was identified in an EMS mutagenesis of 35S::PI transgenic plants in the Nossen ecotype. Plants were grown and maintained as described (*5*).
8. S. E. Clark, R. W. Williams, E. M. Meyerowitz, *Cell* **89**, 575 (1997).
9. B. Kobe and J. Deisenhofer, *Trends Biochem. Sci.* **19**, 415 (1994); S. G. S. C. Buchanan and N. J. Gay, *Prog. Biophys. Mol. Biol.* **65**, 1 (1996).
10. K. A. Feldmann and M. D. Marks, *Mol. Gen. Genet.* **208**, 1 (1987).
11. E. Wisman, G. H. Cardon, P. Fransz, H. Saedler, *Plant Mol. Biol.* **37**, 989 (1998).
12. Genomic DNA flanking the *En-1* insertion site of *clv3-7* was amplified by Tail PCR (polymerase chain reaction) according to standard protocols and used to screen a wild-type Columbia library to identify genomic clones. In addition, a genomic library was made from *clv3-3* plant DNA by Sau 3A partial digestion and ligation into λGEM11 (Promega). The library was screened with T-DNA border sequence probes, and positive clones were hybridized to Southern blots to detect flanking genomic DNA. A single clone containing T-DNA and bordering genomic sequences was used to probe a wild-type Columbia genomic library in λGEM11. Sac I restriction fragments comprising 24 kb of flanking genomic DNA were subcloned into pBluescriptIISK$^+$ (Stratagene), and two subclones containing the *CLV3* region were double-strand sequenced. Nucleotide sequencing was performed with the ABI PRISM Ready Reaction Kit (Perkin-Elmer) and synthetic oligonucleotides on an ABI Automated Cycle Sequencer machine. The entire *CLV3* coding region, plus 800 bp of 5′ sequence and 1 kb of 3′ sequence, was sequenced at least once on each strand. 5′ rapid amplification of cDNA ends (RACE) was performed with primers CLV3B (5′-CTTGGTGGGTTCATCATGATGG) and CLV3C (5′-GTGCAAGGGTCAGGTCC) with the 5′RACE System (Gibco-BRL) according to the manufacturer's protocol. 3′ RACE was performed with primer oli3.6 (5′-GGAAAGTGAATGGGTTGGAGC) according to standard protocols.
13. To identify mutations in the EMS-induced alleles, we amplified the *CLV3* coding region by PCR. PCR products were purified with the QIAquick PCR Purification Kit (Qiagen) and directly sequenced. Products from three independent PCR amplifications were sequenced from each wild-type and mutant genotype.
14. To identify lesions in the *clv3-2* and *clv3-4* alleles, we digested wild-type and mutant genomic DNA with multiple restriction enyzmes and performed Southern blot analysis.
15. G. von Heijne, *Nucleic Acids Res.* **14**, 4683 (1986).
16. K. Nakai and M. Kanehisa, *Genomics* **14**, 897 (1992).
17. R. N. Stewart, in *The Clonal Basis of Development*, S. Subtelny and I. M. Sussex, Eds. (Academic Press, New York, 1978).
18. R. A. E. Tilney-Bassett, *Plant Chimeras* (Arnold, London, 1986).
19. Supplemental Web material is available at www.sciencemag.org/feature/data/ 987103.shl.
20. For nonradioactive in situ hybridization, samples were treated as described [D. Bradley, R. Carpenter, H. Sommer, N. Hartley, E. Coen, *Cell* **72**, 85 (1993)]. For radioactive in situ hybridization, samples were treated as described [H. Sakai, L. J. Medrano, E. M. Meyerowitz, *Nature* **378**, 199 (1995)]. The full-length *CLV3* cDNA cloned in either the sense or antisense orientation relative to the T7 promoter was used as a template for probe synthesis with T7 RNA polymerase.
21. M. K. Barton and R. S. Poethig, *Development* **119**, 823 (1993).
22. D. R. Smyth, J. L. Bowman, E. M. Meyerowitz, *Plant Cell* **2**, 755 (1990).
23. J. A. Long and M. K. Barton, *Development* **125**, 3027 (1998).
24. R. W. Williams and E. M. Meyerowitz, personal communication.
25. P. Becraft, *Trends Plant. Sci.* **3**, 384 (1998).
26. We thank E. Wisman, B. Williams, and S. Jacobsen for *clv3* alleles, the *Arabidopsis* Biological Resource Center at Ohio State University for seeds, J. Wong and N. Beinert for technical assistance, B. Williams for sharing unpublished data, and members of the Meyerowitz Lab for discussion. This work was supported by the U.S. National Institutes of Health (J.C.F.), the Howard Hughes Medical Institute (M.P.R.), the Deutsche Forschungsgemeinschaft (SFB 243, R.S. and U.B.), the National Science Foundation (E.M.M.), and Zeneca Seeds (E.M.M.).

15 December 1998; accepted 24 February 1999

Crystal Structure of Human ZAG, a Fat-Depleting Factor Related to MHC Molecules

Luis M. Sánchez,[1]* Arthur J. Chirino,[1,2]* Pamela J. Bjorkman[1,2]†

Zn-α_2-glycoprotein (ZAG) is a soluble protein that is present in serum and other body fluids. ZAG stimulates lipid degradation in adipocytes and causes the extensive fat losses associated with some advanced cancers. The 2.8 angstrom crystal structure of ZAG resembles a class I major histocompatibility complex (MHC) heavy chain, but ZAG does not bind the class I light chain β_2-microglobulin. The ZAG structure includes a large groove analogous to class I MHC peptide binding grooves. Instead of a peptide, the ZAG groove contains a nonpeptidic compound that may be implicated in lipid catabolism under normal or pathological conditions.

ZAG is a soluble protein whose name derives from its tendency to precipitate with zinc salts and its electrophoretic mobility in the region of the α_2 globulins (*1*). ZAG is normally present in most body fluids including serum, sweat, saliva, cerebrospinal fluid, seminal plasma, milk, amniotic fluid, and urine (*1*). In addition, ZAG accumulates in breast cysts as well as in 40% of breast carcinomas, and is induced by glucocorticoids and androgens in breast cancer cell lines. Hence, ZAG may participate in breast diseases, including cancer (*2*).

The function of ZAG was elucidated when a lipid-catabolizing factor with the same amino acid sequence as ZAG was isolated from the urine of cancer patients with cachexia (*3*). Cachexia is a wasting syndrome caused by depletion of muscle and adipose tissue that is present in the majority of patients with cancer, AIDS, and other life-threatening diseases (*3*). ZAG appears to be responsible for the fat-depletion component of cachexia, since it stimulates lipid breakdown in adipocytes and reduces fat stores in laboratory animals (*3*). ZAG is overexpressed in carcinomas that induce fat loss but not in other tumors. Application of ZAG to adipocyte membranes activates a guanosine triphosphate–dependent adenylate cyclase activity, perhaps through direct or indirect interactions with a G protein–coupled receptor (*3*). Thus, its mode of action could be similar to that of lipolytic hormones. These results suggest that ZAG normally functions to regulate lipid degradation, which increases to a pathological extent in cachexia.

ZAG shares 30 to 40% amino acid sequence identity with the extracellular portions of class I major histocompatibility complex (MHC) heavy chains (*4*). Class I MHC molecules present peptide antigens to cytotoxic T cells (*5*). Other proteins related to class I MHC molecules include CD1, which presents hydrophobic antigens to T cells (*6*), the neonatal Fc receptor (FcRn), which transports immunoglobulin G across epithelia (*7*), and HFE, which binds transferrin receptor and regulates iron homeostasis (*8*). These MHC homologs are membrane-bound heterodimers that use the soluble protein β_2-microglobulin (β_2M) as a light chain. ZAG, however, is a secreted protein, and it does not associate with β_2M (*9*). The latter property is shared by MIC-A, a divergent membrane-bound member of the class I family (*10*).

Like FcRn (*11*), HFE (*11*), and MIC-A (*10*), ZAG does not bind endogenous peptides (*9*), but it appears to carry a small proteinase-resistant compound whose injection induces glomerulonephritis in experimental animals (*12*). In peptide-binding class I MHC molecules, a large groove located between two α helices in the α1-α2 superdomain of the heavy chain serves as the binding site (*5*). An analogous groove acts as the antigen binding site in CD1,

[1]Division of Biology 156-29 and [2]Howard Hughes Medical Institute, California Institute of Technology, Pasadena, CA 91125, USA.

*These authors contributed equally to this work.
†To whom correspondence should be addressed. E-mail: bjorkman@cco.caltech.edu